sciendo

Straight and Bent Bars Buckling Considered as the Axial Displacement of One Bar End

doi:10.2478/mape-2020-0005
Date of submission to the Editor: 03/2020
Date of acceptance by the Editor: 06/2020
MAPE 2020, volume 3, issue 1, pp. 57-70

Stefan Berczyński
ORCID ID: 0000-0002-8403-6355

Paweł Dunaj
ORCID ID: 0000-0001-6866-2586
West Pomeranian University of Technology, **Poland**

Zenon Grządziel
ORCID ID: 0000-0001-9348-1111
Maritime University of Szczecin, **Poland**

INTRODUCTION

Buckling is a classic mechanical problem, the concept of which was introduced by Euler (Euler, 1744). Over the years, buckling analysis has found wide application, including in civil engineering (Śledziewski & Górecki, 2020; Toledo et al., 2020), mechanical engineering (Czechowski et al., 2020; Kubit et al., 2019) or the maritime industry (Corigliano et al., 2019; Shen et al., 2020). Currently, there is a renewed interest in buckling, in particular in applications in composite structures (Rozylo et al., 2020; Schilling & Mittelstedt, 2020; Xu & Wu, 2008) or micro and nano technologies (Barretta et al., 2019; Chandra et al., 2020). A large number of industrial applications and scientific research (Li & Batra, 2013; Nistor et al., 2017) of buckling analysis have resulted in the development of buckling modeling methods.

In (Harvey & Cain, 2020) authors investigated column behavior if member imperfection and load eccentricity are simultaneously present. Authors analyzed pinned members assuming linearly elastic, slender, uniform, and inextensible columns. To compare the relative significance of member imperfections and load eccentricity on the deflected shape a linear analysis based on Euler-Bernoulli theory was performed. The obtained results were experimentally validated using additively manufactured specimen. Additive manufacturing ensured accurate seeding imperfections to control, specimens buckling characteristics. A series of initially imperfect specimens with eccentric load application points were tested, exhibiting imperfection amplification and cancellation. Authors stated that good agreement between the theoretical predictions and the experimental results was observed.

In (Zhu et al., 2017) author presented, an analytical study on the buckling problem of nonlocal Euler-Bernoulli beams using Eringen's two-phase nonlocal

Contact address: z.grzadziel@am.szczecin.pl

integral model (Eringen, 2002). Authors deduced the exact characteristic equation for the buckling loads, by the reduction method. In addition, a simple and explicit expressions of the buckling loads for four-type boundary conditions was developed. Authors proved that adopted nonlocal integral model has a consistent softening, in contrast to the nonlocal differential model. Authors stated that in comparison with differential model and the pure nonlocal model, the integral model considered advantages of well-posedness and self-consistency. In addition, the established analytical formulae may be useful in providing guidelines for designing structures with nonlocal effect, since they contain the nonlocal parameter explicitly.

In (Su et al., 2019) authors presented a finite prebuckling deformation (FPD) buckling theory to analyze the FPD buckling behaviors of beams with the coupling of bending, twist and stretch/compression. To verify the correctness of the proposed theory, it was compared with various analytical and numerical methods of modeling the transverse buckling of a three-point bending beam, lateral buckling of pure beam bending and Euler buckling. In result, it was stated than proposed FPD buckling theory for beams is able to give a good prediction, while the conventional buckling theory (Timoshenko & Gere, 2009) and conventional numerical method (Dassault-Systèmes, 2010) yield unacceptable results (in some cases with 70% error for a three-point-bending beam).

In (Nikolić & Šalinić, 2017) authors presented a method of buckling analysis of non-prismatic columns based on rigid element method. Authors derived a general form of the characteristic equation, which enabled to perform buckling analysis of columns with continuously varying, doubly symmetric cross-section and multiple-stepped columns under different boundary conditions. The proposed method was verified through numerical examples. Authors concluded that results obtained on the basis of presented method have a high rate of convergence to the other results from the literature.

Summing up the presented review of buckling analysis methods, it can be stated that despite the fact that buckling is a classic problem of mechanics, researchers are constantly proposing new approaches to solve this problem, as a result of which they determine the values characterizing buckling. One such approach is proposed in this article. Presented approach deals with the problem determining specific buckling amplitude of straight and bent bar, where it is considered as a function of axial displacement of one end of the bar. The main novelty is that assumption that the length of a buckled bar at any instant of buckling is the same as that of a straight bar, regardless of the size of axial displacement of one end of the bar. A formula for the value of axial displacement of one bar end or buckling amplitude in the middle of bar length as a function of compressive force was derived – based on energy equations. The proposed method was validated for bars with different cross-section dimensions by comparing results obtained on its basis with finite element model results and experimental tests.

The structure of the article is as follows: in Section 2, the proposed method of determining axial displacement of one bar end or buckling amplitude in the

middle of bar length presented. Next, the results obtained on the basis of presented method are compared to finite element model and experimental test results. In Section 4, a discussion of the results obtained is provided. Section 5 contains the final conclusions that summarize the most important achievements of the article.

METHODOLOGY OF RESEARCH

Euler bar buckling

Bending a bar caused by exceeding a critical value of axial compressive force is called buckling. The value of this critical force was determined by Euler (Bedford & Liechti, 2020; Euler, 1744; Gere & Goodno, 2009; Timoshenko & Gere, 2009). He considered the equilibrium of a bent bar (Fig. 1).

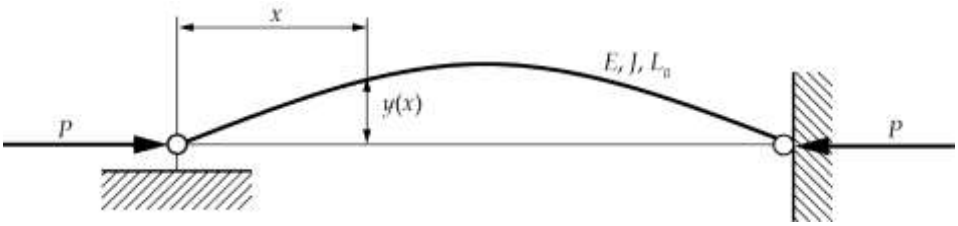

Fig. 1 Equilibrium of a bent bar, *E* – Young modulus, *J* – axial moment of inertia of bar cross-section, L_0 – initial length of straight bar

Solving the differential equation, Euler derived a well-known formula for the value of critical force:

$$P = \frac{\pi^2 EJ}{L_0^2} \tag{1}$$

The bent axis of the bar is a sinusoid:

$$y(x) = A \cdot sin\ \left(\frac{\pi x}{L_0}\right) \tag{2}$$

Amplitude *A* at the bar half-length can be written:

$$y\ \left(\frac{L_0}{2}\right) = A \tag{3}$$

However, a specific value of amplitude A at such approach to buckling cannot be determined.

Model of straight bar buckling under axial displacements δ of one end of the bar

The article aims to determine the course of axial displacement δ of one bar end (or amplitude *A* of buckling, measured at half-length of the bar) as the function of axial compressive force *P.* A model of buckling due to axial displacements δ of one bar end is presented (Fig. 2). It can be compared to a bar placed in the closing jaws of a vice. Axial forces occur then as reaction forces in the supports (jaws).

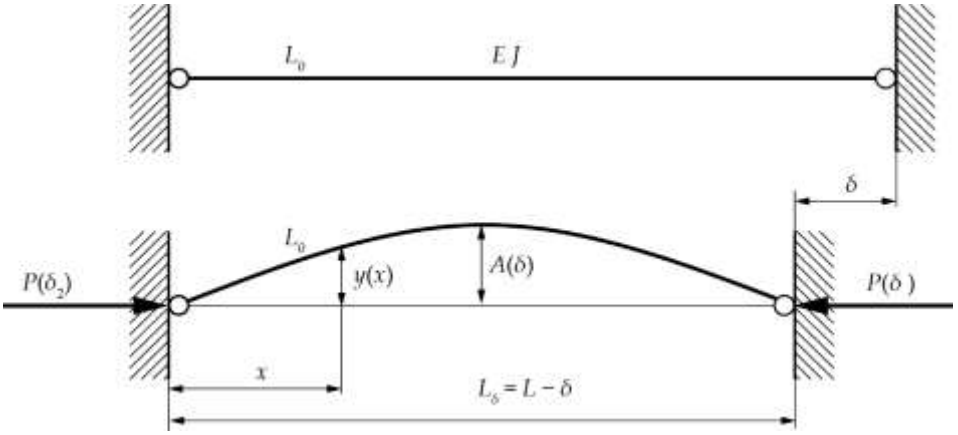

Fig. 2 Buckling of a bar with a specific initial length L_0 at preset axial displacement δ of one end

It was assumed that the bent bar has a shape of a sinusoid with amplitude *A*, at a length between the supports shortened by displacement *δ*:

$$y(x) = A \cdot sin\ \left(\frac{\pi \cdot x}{L_0 - \delta}\right) \tag{4}$$

To determine the relationship between amplitude *A* and a preset axial displacement *δ*, we need to know the formula for the length of the sinusoid. The sinusoid length for each value must be equal to the initial straight bar length L_0. The length of the sinusoid cannot be determined by elementary functions. A precise formula for the length of the sinusoid:

$$L_0 = 2 \cdot a \cdot E\ (e^2) \tag{5}$$

where:

E is a complete elliptic integral of the second kind, *e* is an eccentricity of an ellipse.

Elliptic integrals were encountered while calculating the ellipse circumference, hence their name. The term refers to integrals that cannot be expressed by elementary functions. We can imagine a sinusoid as an expansion of an ellipse formed by an intersection of a cylinder by a plane at a certain angle to the axis and passing through the diameter of this cylinder (Fig. 3a) (Czechowski et al., 2020; Kubit et al., 2019).

Half of the ellipse circumference is the sinusoid length. An approximate formula for ellipse length *L*:

$$L \approx \pi \cdot \left(\frac{3}{2} \cdot (a + b) - \sqrt{a \cdot b}\right) \tag{6}$$

where:

a, *b* are a semi-axes of an ellipse.

It follows from Figure 3b that

$$y(x) = a \cdot sin\,\alpha \cdot tan\,\gamma \tag{7}$$

where:

a is a smaller minor semi-axis, equal to the radius of the cylinder from which the ellipse is expanded,

γ is a dihedral angle between the ellipse plane and a plane perpendicular to the cylinder axis.

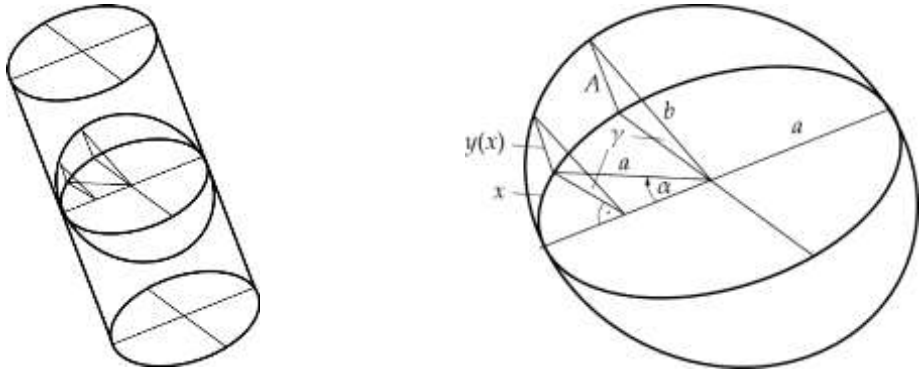

(a) **(b)**

Fig. 3 (a) An ellipse formed by intersection of a cylinder by a plane at a certain angle to the cylinder axis, passing through the diameter of this cylinder; (b) relationships between a cylinder with diameter 2·*a* and an ellipse with semi-axes and a sinusoid with an amplitude *A*

As the minor semi-axis *a* and the dihedral angle *γ* are constant, equation *y(x)* represents a sinusoid. It follows from Figure 3b that the minor semi-axis *a* of the ellipse equals the radius of the cylinder with circumference length $2 \cdot L_\delta$:

$$2 \cdot L_\delta = 2 \cdot (L_0 - \delta) = \pi \cdot 2 \cdot a \rightarrow a = \frac{L_0 - \delta}{\pi} \tag{8}$$

The major semi-axis *b* results from the initial length L_0 of the bar, equal to half the circumference of the ellipse:

$$L_0 = \frac{\pi}{2} \cdot \left(\frac{3}{2} \cdot (a + b) - \sqrt{a \cdot b} \right) \tag{9}$$

In further steps, the attention will be focused on the determination of the major axis *b* from the above equation. After simple transformations:

$$\frac{2 \cdot L_0}{\pi} = \frac{3}{2} \cdot a + \frac{3}{2} \cdot b - \sqrt{a \cdot b} \tag{10}$$

$$-\frac{2 \cdot L_0}{\pi} + \frac{3}{2} \cdot a + \frac{3}{2} \cdot b = \sqrt{a \cdot b} \tag{11}$$

we temporarily adopt a constant value *D*:

$$D = -\frac{2 \cdot L_0}{\pi} + \frac{3}{2} \cdot a \tag{12}$$

Then

$$\left(D + \frac{3}{2} \cdot b \right)^2 = a \cdot b \tag{13}$$

We remove the brackets:

$$D^2 + 2 \cdot D \cdot \frac{3}{2} \cdot b + \frac{9}{4} \cdot b^2 = a \cdot b \tag{14}$$

to get a square trinomial:

$$\frac{9}{4} \cdot b^2 + (3 \cdot D - a) \cdot b + D^2 = 0 \tag{15}$$

The discriminant of the trinomial:

$$\Delta = (3 \cdot D - a)^2 - 4 \cdot \frac{9}{4} \cdot D^2 = a^2 - 6 \cdot D \cdot a \tag{16}$$

The roots $b_{1,2}$ of the equation

$$b_{1,2} = \frac{-(3 \cdot D - a) \pm \sqrt{a^2 - 6 \cdot D \cdot a}}{2 \cdot \frac{9}{4}} \tag{17}$$

After the rejection of the unreal solution, the only real solution is

$$b = \frac{-6 \cdot D + 2 \cdot a + 2 \cdot \sqrt{a^2 - 6 \cdot D \cdot a}}{9} \tag{18}$$

Replacing *D* by the previous value, we get

$$b = \frac{-6\cdot\left(-\frac{2\cdot L_0}{\pi}+\frac{3}{2}a\right)+2\cdot a+2\cdot\sqrt{a^2-6\cdot\left(-\frac{2\cdot L_0}{\pi}+\frac{3}{2}\cdot a\right)\cdot a}}{9} \quad (19)$$

After the reduction of the brackets:

$$b = \frac{\frac{12\cdot L_0}{\pi}-7\cdot a+2\cdot\sqrt{\frac{12\cdot L_0\cdot a}{\pi}-8\cdot a^2}}{9} \quad (20)$$

The final form of the major semi-axis *b* expressed by the minor semi-axis *a*:

$$b = \frac{4\cdot L_0}{3\cdot\pi}-\frac{7}{9}\cdot a+\frac{2}{9}\cdot\sqrt{\frac{12\cdot L_0\cdot a}{\pi}-8\cdot a^2} \quad (21)$$

We substitute for *a*: $a = (L_0 - \delta)/\pi$

$$b = \frac{4\cdot L_0}{3\cdot\pi}-\frac{7}{9}\cdot\frac{L_0-\delta}{\pi}+\frac{2}{9\cdot\pi}\cdot\sqrt{4\cdot L_0^2+4\cdot L_0\cdot\delta-8\cdot\delta^2} \quad (22)$$

We introduce the least common denominator:

$$b = \frac{5\cdot L_0}{9\cdot\pi}+\frac{7}{9}\cdot\frac{\delta}{\pi}+\frac{2}{9\cdot\pi}\cdot\sqrt{4\cdot L_0^2+4\cdot L_0\cdot\delta-8\cdot\delta^2} \quad (23)$$

and obtain the final formula for the major semi-axis of the ellipse as the function of one variable δ:

$$b = \frac{1}{9\cdot\pi}\left(5\cdot L_0+7\cdot\delta+2\cdot\sqrt{4\cdot L_0^2+4\cdot L_0\cdot\delta-8\cdot\delta^2}\right) \quad (24)$$

If $\delta = 0$ then $b = L_0/\pi$, i.e. the two semi-axes *a* and *b* are equal and the ellipse becomes a circle. The other root of the square trinomial would be $b = L_0/(9\pi)$ unrealistic, as the major semi-axis *b* would be smaller than the minor semi-axis *a*.

The sinusoid amplitude is expressed by the formula (Fig. 3b):

$$A = \sqrt{b^2-a^2} \quad (25)$$

$$A = \sqrt{\left[\frac{1}{9\cdot\pi}\left(5\cdot L_0+7\cdot\delta+2\cdot\sqrt{4\cdot L_0^2+4\cdot L_0\cdot\delta-8\cdot\delta^2}\right)\right]^2-\left(\frac{L_0-\delta}{\pi}\right)^2} \quad (26)$$

The ultimate equation of the sinusoid:

$$y(x) = A\cdot sin\left(\frac{\pi\cdot x}{L_\delta}\right) \quad (27)$$

By knowing the sinusoid equation, we can determine the elastic energy U_S accumulated in the bar (Shen et al., 2020):

$$U_S = \frac{1}{2}\int_0^{L_\delta} E\cdot J\cdot y''^2 dx \quad (28)$$

replacing:

$$\omega = \frac{\pi}{L_\delta} \quad (29)$$

$$y(x) = A\cdot sin(\omega\cdot x) \quad (30)$$

$$y'(x) = A\cdot\omega\cdot cos\ \ (\omega\cdot x) \quad (31)$$

$$y''(x) = -A\cdot\omega^2\cdot sin\ \ (\omega\cdot x) \quad (32)$$

Elastic energy U_S in the bar caused by bending:

$$U_S = \frac{1}{2}\int_0^{L_\delta} E\cdot J\cdot y''^2 dx = \frac{1}{2}\int_0^{L_\delta} E\cdot J\cdot A^2\cdot\omega^4\cdot sin^2(\omega\cdot x) \rightleftarrows\ dx = \frac{E\cdot J\cdot A^2\cdot\omega^4}{2}\int_0^{L_\delta} sin^2(\omega\cdot x) \rightleftarrows\ dx = = \frac{E\cdot J\cdot A^2\cdot\omega^3}{2}\cdot\frac{1}{2\omega}\cdot[\omega\cdot x-sin(\omega\cdot x)\cdot cos(\omega\cdot x)]_0^{L_\delta} \quad (33)$$

$$U_S = \frac{E\cdot J\cdot A^2\cdot\left(\frac{\pi}{L_\delta}\right)^3}{4}\cdot\left[\frac{\pi}{L_\delta}\cdot x-sin\left(\frac{\pi}{L_\delta}\cdot x\right)\cdot cos\left(\frac{\pi}{L_\delta}\cdot x\right)\right]_0^{L_\delta} = \frac{E\cdot J\cdot A^2\cdot\pi^4}{4\cdot L_\delta^3} \quad (34)$$

An increment of elastic energy ΔU_S accumulated in the bar along with an increment of displacement $\Delta\delta$ is equal to work ΔU_p of the external compressive force *P* over a distance of axial increment of displacement $\Delta\delta$:

$$\Delta U_S = \Delta U_P \tag{35}$$

$$\frac{E \cdot J \cdot \pi^4}{4} \cdot \left(\frac{A_\delta^2}{L_\delta^3} - \frac{A_{\delta-\Delta\delta}^2}{L_{\delta-\Delta\delta}^3} \right) = P \cdot \Delta\delta \tag{36}$$

Hence the value of the compressive force *P*:

$$P = \frac{E \cdot J \cdot \pi^4}{4} \cdot \left(\frac{A_\delta^2}{L_\delta^3} - \frac{A_{\delta-\Delta\delta}^2}{L_{\delta-\Delta\delta}^3} \right) \cdot \frac{1}{\Delta\delta} = C \cdot \left(\frac{A_\delta^2}{L_\delta^3} - \frac{A_{\delta-\Delta\delta}^2}{L_{\delta-\Delta\delta}^3} \right) \cdot \frac{1}{\Delta\delta} \tag{37}$$

where the constant *C*:

$$C = \frac{E \cdot J \cdot \pi^4}{4} \tag{38}$$

The verifying calculations were made for the following theoretical data: L = 750 mm, $E = 2.07 \cdot 10^5$ MPa, J = 1250 mm^3

$$P_{\text{kr}} = \frac{\pi^2 EJ}{L^2} = 4540 \ N \quad \text{(Euler)} \tag{39}$$

The calculations of the previously discussed quantities *a*, *b*, *A*, U_S, *P* were made, depending on the stepwise changing value of the axial displacement *δ*. At the start of the compression, the bar was perfectly straight. The results of the calculations are contained in Table 1.

Table 1 The values *a*, *b*, *A*, U_S, *P* depending on the stepwise variable value of the axial displacement *δ*

Displacement	Minor axis	Major axis	Sinusoid amplitude	Elastic energy	Force compressing initially straight bar
d [Nm]	*a* [Nm]	*b* [Nm]	*A* [Nm]	U_S [Nmm]	*P* [N]
0	238.7324	238.7324	0.00	0	0
0.00114	238.7321	238.7328	0.59	5	4540
0.00228	238.7317	238.7331	0.83	10	4540
0.00342	238.7313	238.7335	1.02	16	4540
0.00456	238.7310	238.7339	1.18	21	4540
0.0057	238.7306	238.7342	1.32	26	4540
0.00684	238.7302	238.7346	1.44	31	4540
0.00798	238.7299	238.7350	1.56	36	4540
0.00912	238.7295	238.7353	1.66	41	4540
0.01026	238.7291	238.7357	1.77	47	4540
0.0114	238.7288	238.7360	1.86	52	4540
0.01254	238.7284	238.7364	1.95	57	4540
0.01368	238.7281	238.7368	2.04	62	4540
0.01482	238.7277	238.7371	2.12	67	4540
0.01596	238.7273	238.7375	2.20	72	4541
0.0171	238.7270	238.7379	2.28	78	4541
0.01824	238.7266	238.7382	2.35	83	4541
0.01938	238.7262	238.7386	2.43	88	4541
0.02052	238.7259	238.7389	2.50	93	4541

The diagram of axial displacement *δ* as the function of axial compressive force *P* for this case is presented in Figure 4a.

This is a vertical line intersecting the horizontal axis (axis of force) at the critical force value according to Euler. The amplitude *A* graph at half-length of the bar perpendicular to the bar axis as the function of the axial compressive force *P* for this case is presented in Figure 4b.

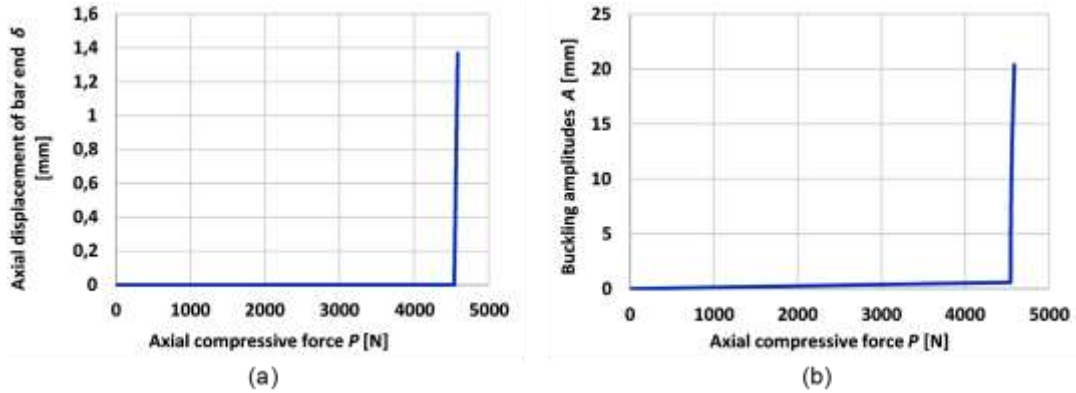

Fig. 4 Axial displacements δ of bar end (a) and the graph of amplitudes A = A(δ) of the bar buckling at the bar half-length (b) as the function of axial compression force P

It is also a vertical line intersecting the horizontal axis at the identical value of the critical force according to Euler. Analytically, the value of this asymptote can be easily expressed by the formula obtained by the substitution to force *P* of a small value of displacement equal to, e.g.

$$\delta = 0.01 \text{ mm} = 1 \cdot 10^{-5} \cdot L_0 \text{ mm} \tag{40}$$

The minor semi-axis:

$$a = \frac{L_0 - \delta}{\pi} = \frac{L_0 - 1 \cdot 10^{-5} \cdot L_0}{\pi} = \frac{0.99999}{\pi} \cdot L_0 \tag{41}$$

The major semi-axis:

$$b = \frac{1}{9 \cdot \pi}\left(5 \cdot L_0 + 7 \cdot \delta + 2 \cdot \sqrt{4 \cdot L_0^2 + 4 \cdot L_0 \cdot \delta - 8 \cdot \delta^2}\right) \tag{42}$$

$$b = \frac{1}{9 \cdot \pi}\left(5 \cdot L_0 + 7 \cdot 10^{-5} \cdot L_0 + 2 \cdot \sqrt{4 \cdot L_0^2 + 4 \cdot L_0 \cdot 10^{-5} \cdot L_0 - 8 \cdot (10^{-5} \cdot L_0)^2}\right) \tag{43}$$

$$b = \frac{1.00001}{\pi} \cdot L_0 \tag{44}$$

Amplitude *A*:

$$A = \sqrt{b^2 - a^2} = \frac{L_0}{\pi} \cdot 0.006325 \tag{45}$$

$$P = \frac{E \cdot J \cdot A^2 \cdot \pi^4}{4 \cdot L_\delta^3 \cdot \delta} = \frac{\pi^4 \cdot E \cdot J \cdot L_0^2 \cdot 0.006325^{\,2}}{\pi^2 \cdot 4 \cdot 0.99999^3 \cdot L_0^3 \cdot 0.00001 \cdot L_0} = \frac{\pi^2 \cdot E \cdot J}{L_0^2} \cdot \frac{4 \cdot 10^{-4}}{4 \cdot 10^{-4}} \tag{46}$$

$$P = \frac{\pi^2 \cdot E \cdot J}{L_0^2} \tag{47}$$

The above value is identical to the value of the critical force determined by the Euler formula. Therefore, a graph of axial displacement δ of one bar end was obtained as the function of axial compression force *P* as well as a graph of buckling amplitude *A* at bar half-length as the function of the axial compression force *P*, which was the objective of this article.

Model of bent bar buckling under axial displacements δ of one end of the bar

If we assume the bar is initially bent $A(\delta_0)$, which can be regarded as initial displacement δ_0 of the bar end by value δ_0 (Fig. 5) (we omit elastic strains caused by compressive stresses), then the elastic energy of the strain U_S caused by further movement of the bar end must be expressed by the difference of amplitudes $A = A(\delta) - A(\delta_0)$ (Fig. 5).

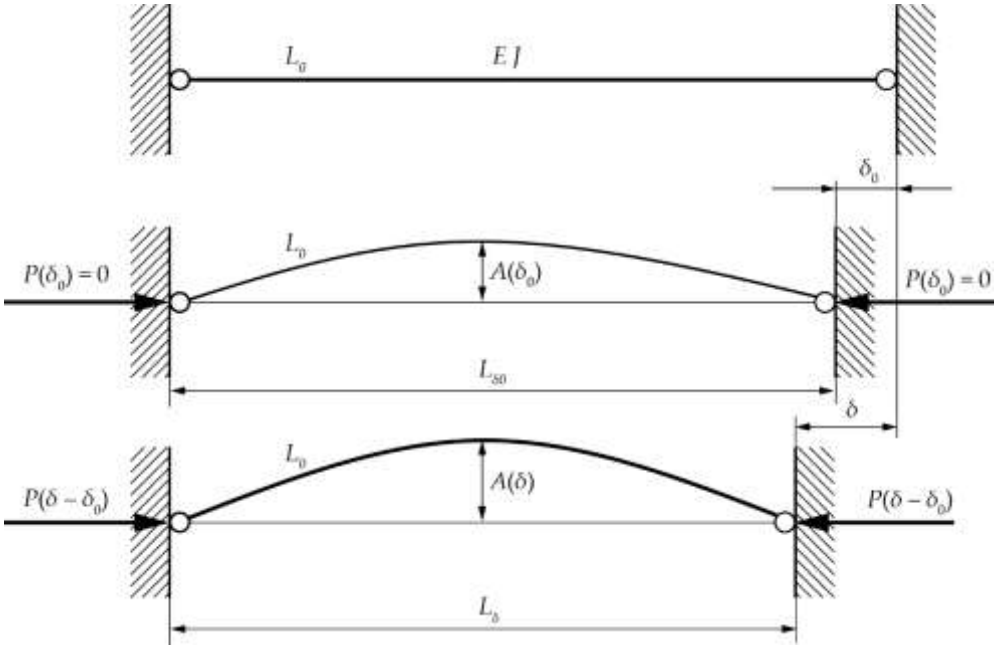

Fig. 5 Preliminary bending of the bar due to initial displacement of bar end by value δ_0

$$U_S = \frac{E \cdot J \cdot \left(A(\delta) - A(\delta_0)\right)^2 \cdot \pi^4}{4 \cdot L_\delta^3} \tag{48}$$

and the value of the compressive force P:

$$P = C \cdot \left(\frac{[A(\delta) - A(\delta_0)]^2}{L_\delta^3} - \frac{[A_{\delta-\Delta\delta} - A(\delta_0)]^2}{L_{\delta-\Delta\delta}^3} \right) \cdot \frac{1}{\Delta\delta} \tag{49}$$

This case of buckling was calculated for the initial value of the bar end displacement δ_0 according to Table 2.

Table 2 Initial values δ_0 of the bar end displacement and the corresponding initial amplitude $A(\delta_0)$ of the bar bent at half-length. $\Delta\delta$ – stepwise displacement of bar end

Initial displacement of bar end [mm]	Initial bending of the bar at its half-length [mm]	Stepwise displacement of bar end [mm]
δ_0	$A(\delta_0)$	$\Delta\delta$
0.00002850	0.0931	0.00002850
0.002850	0.931	0.002850
0.01425	2.08	0.00285
0.03135	3.09	0.00285

The results of the calculations for four initial displacements δ_0 of the bar end according to Table 2 are presented in Figures 9 and 10.

A simplified buckling model of a bent bar

In this approach only buckling amplitudes are considered. This method of determining the critical force is commonly used in lab classes on buckling (Buczkowski & Banaszek, 2006). The amplitude increment in a bar $A = A(\delta) - A(\delta_0)$ initially bent at its half-length by a value $A(\delta_0)$ is determined with sufficient accuracy by means of the approximate formula (Buczkowski & Banaszek, 2006):

$$A = A(\delta) - A(\delta_0) = \frac{A(\delta_0)}{\frac{P_{kr}}{P}} - 1 \tag{50}$$

Hence

$$P = \frac{P_{kr}}{\frac{A(\delta_0)}{A(\delta) - A(\delta_0)} + 1} \tag{51}$$

The graph of this approximate value of amplitude $A = A(\delta) - A(\delta_0)$ increment as the function of axial compressive force P is presented for $A(\delta_0) = 0.59$ mm in Figure 8a.

Finite element model

Simulation calculations were made using the Midas NFX 2018 R1 preprocessor (Midas Information Technology Co. Ltd., Seongnam, Korea) (Midas, 2011) computer program based on the finite element method. The modeled bar had dimensions as given in the previous section. The one-dimensional finite beam elements (CBEAM) were used. The finite element model was composed of 81 nodes and 80 elements. The bar ends were modeled as hinged support, and one end had a preset axial displacement $\delta = -1$mm (Fig. 6).

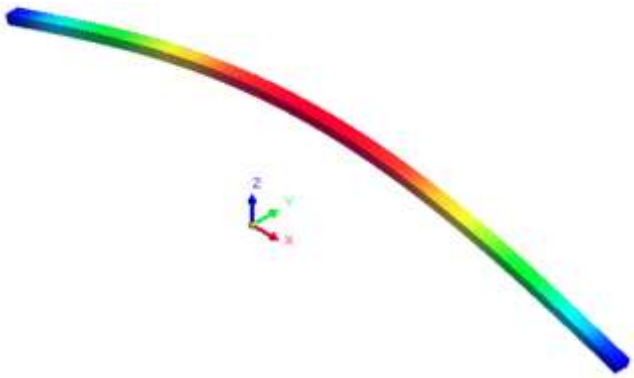

Fig. 6 Diagram of the computer model of a compressed bar

The non-linear static module (SOL 106) was used for the calculations. Further in this study the initial axial displacement δ was calculated according to Table 2. The simulation results are shown in Figures 8 to 10, denoted by FEM (Finite Element Method).

Experimental tests

Experimental buckling tests were conducted for a steel bar with dimensions as given in the previous section. The initial amplitude A_0 was 0.59 mm. The value P of the axial force compressing the bar and amplitude A of buckling measured with a micrometer at bar half-length perpendicularly to the bar axis (Fig. 7).

Fig. 7 A bar examined for buckling on a strength tester FM 2500

The experiment results are given in Figure 8.

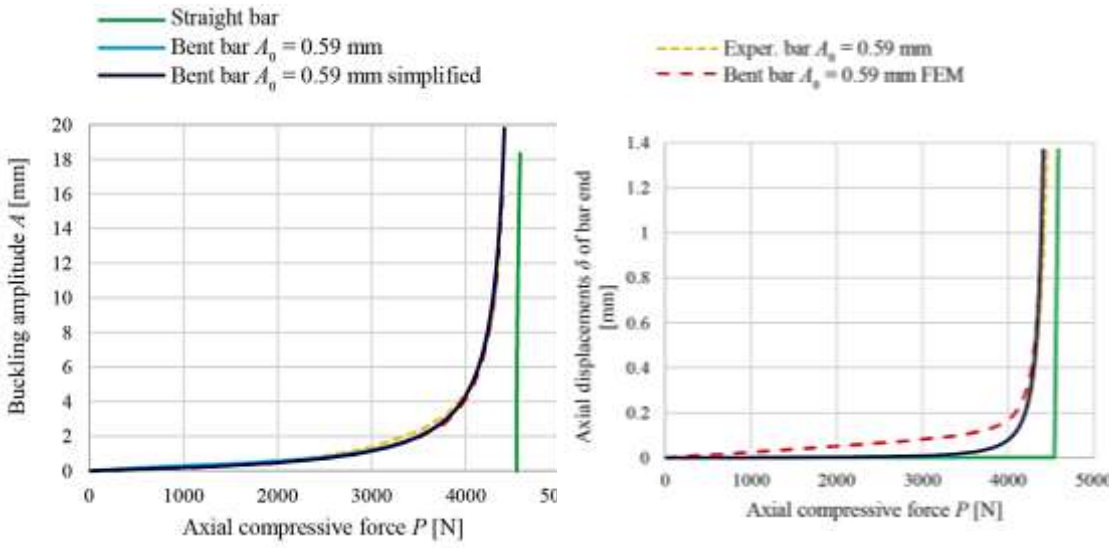

(a) **(b)**

Fig. 8 (a) Buckling amplitudes *A* as a function of compressive forces acting on a bar 750 mm in length, rectangular cross-section 10 x 15 mm, initial buckling amplitude A_0 = 0.59 mm; (b) axial displacements of bar end *δ* as a function of compressive forces acting on a bar 750 mm long, rectangular section 10 x 15 mm, initial value of axial displacement δ_0 = 0.00114 mm

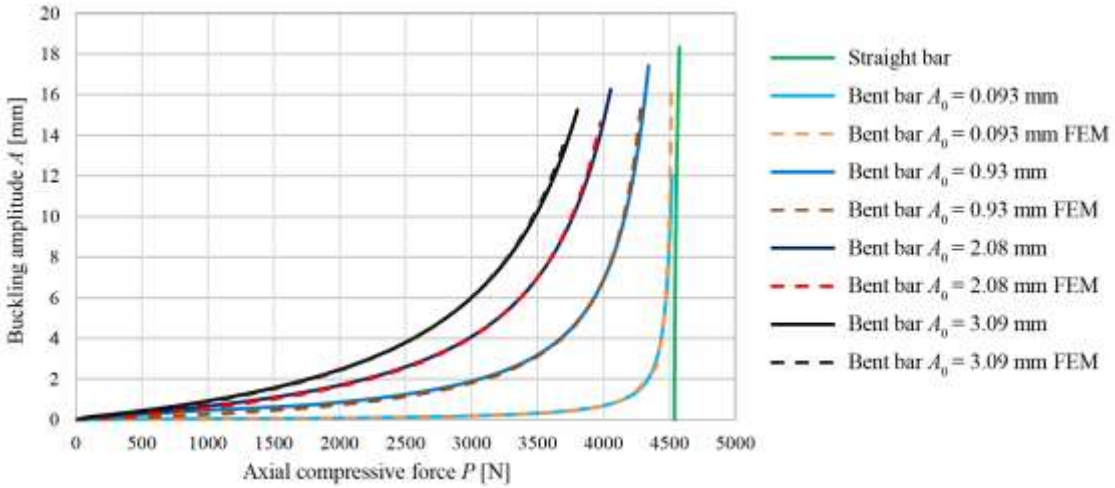

Fig. 9 Analytical and simulation graphs of buckling amplitudes *A* as a function of compressive forces acting on a bar 750 mm in length, rectangular cross-section 10 x 15 mm, various amplitudes A_0 of initial bending

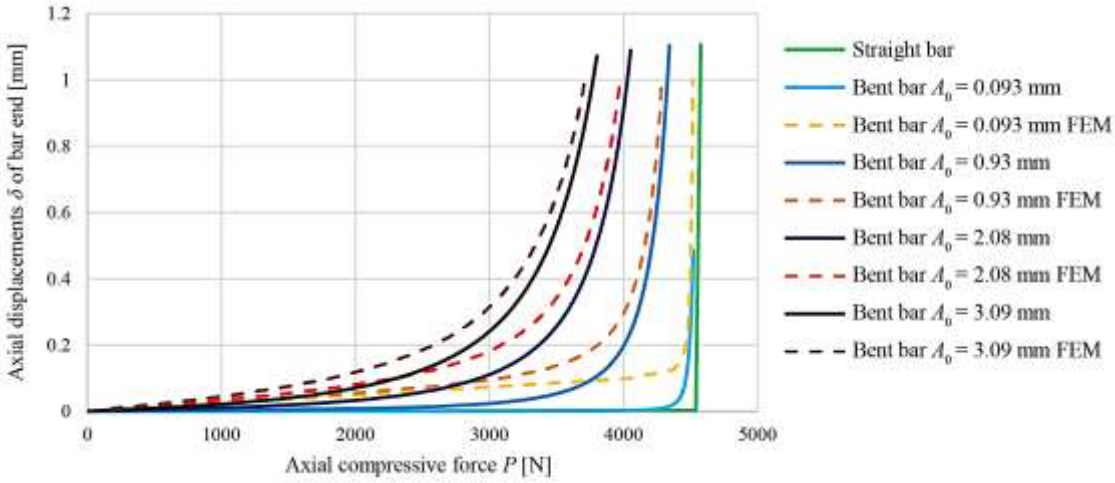

Fig. 10 Analytical and simulation graphs of axial displacement *δ* as a function of axial compression forces, acting on a bar 750 mm in length, rectangular section 10 x 15 mm, for various amplitudes A_0 of initial bending

DISCUSSION

Summarizing the research presented in this article, the experimental studies show, that:

- In a wide range of straight bar end axial displacement *δ* (Fig. 4a) and amplitudes *A* (Fig. 4b) the compressive force *P* is constant and equal to Euler's critical force (Euler, 1744; Timoshenko & Gere, 2009);
- The more the bar is bent at the initial compression stage, the more flattened are the graphs illustrating axial displacement *δ* (Fig. 10) and buckling amplitude *A* (Fig. 9);
- The asymptotic character of axial displacement *δ* of a straight bar end *A* (Fig. 10) and its amplitudes *A* (Fig. 9) as the function of axial compression forces is evident for compressive forces close to the value of Euler's critical force;

- The amplitude graphs differ slightly for the four methods: analytical, simulation, approximate and experimental (Fig. 8a);
- The analytical and simulation graphs of axial displacements δ of the bar end (Fig. 3a) are significantly different in the first phase of compression, but they have a joint asymptote;
- The conformity of amplitude A graphs (Fig. 9) as a function of axial compressive forces obtained by three methods confirms the correct approach to the bar buckling problem by considering the axial displacement of one end of the bar.

CONCLUSIONS

Presented article deals with the problem of straight and bent bar buckling, where bar buckling is considered as a function of axial displacement of one end. Owing to the derived formula it was possible to determine a specific value of amplitude A, which is not possible using Euler method. Obtained results (buckling amplitude and axial displacement of bar end for bars with different cross-section dimensions.) show high agreement with FEM analysis and experimental results.

REFERENCES

Barretta, R., Fabbrocino, F., Luciano, R., de Sciarra, F. M., & Ruta, G. (2019). Buckling loads of nano-beams in stress-driven nonlocal elasticity. *Mechanics of Advanced Materials and Structures*, pp. 1-7.

Bedford, A., & Liechti, K. M. (2020). Buckling of Columns. In *Mechanics of Materials* (pp. 729-781). Springer International Publishing. https://doi.org/10.1007/978-3-030-22082-2_10

Buczkowski, R., & Banaszek, A. (2006). *Mechanika ogólna w ujęciu wektorowym i tensorowym: Statyka: Przykłady i zadania*. Wydawnictwa Naukowo-Techniczne.

Chandra, Y., Flores, E. S., & Adhikari, S. (2020). Buckling of 2D nano hetero-structures with moire patterns. *Computational Materials Science*, 177, 109507.

Corigliano, P., Crupi, V., & Guglielmino, E. (2019). Mechanical buckling analysis of explosive welded joints used in shipbuilding. *International Shipbuilding Progress*, 66(1), pp. 17-34.

Czechowski, L., Kędziora, S., & Kołakowski, Z. (2020). The Buckling and Post-Buckling of Steel C-Columns in Elevated Temperature. *Materials*, 13(1), 74.

Dassault-Systèmes. (2010). *Abaqus Analysis User's Manual v.6.10*. Dassault Systèmes Simulia Corp.

Eringen, A. C. (2002). *Nonlocal continuum field theories*. Springer Science & Business Media.

Euler, L. (1744). *Methodus inveniendi lineas curvas maximi minimive proprietate gaudentes*. apud Marcum-Michaelem Bousquet.

Gere, J. M., & Goodno, B. J. (2009). Mechanics of materials. Cengage learning. *Inc.: Independence, KY*.

Harvey, P. S., & Cain, T. M. N. (2020). Buckling of elastic columns with initial imperfections and load eccentricity. *Structures*, *23*, pp. 660-664. https://doi.org/10.1016/j.istruc.2019.09.021

Kubit, A., Trzepiecinski, T., Święch, Ł., Faes, K., & Slota, J. (2019). Experimental and Numerical Investigations of Thin-Walled Stringer-Stiffened Panels Welded with RFSSW Technology under Uniaxial Compression. *Materials*, 12(11), 1785.

Li, S.-R., & Batra, R. C. (2013). Relations between buckling loads of functionally graded Timoshenko and homogeneous Euler-Bernoulli beams. *Composite Structures*, *95*, 5–9. https://doi.org/10.1016/j.compstruct.2012.07.027

Midas, I. T. (2011). User's Manual of midas NFX. *MIDAS IT*.

Nikolić, A., & Šalinić, S. (2017). Buckling analysis of non-prismatic columns: A rigid multibody approach. *Engineering Structures*, 143, pp. 511-521. https://doi.org/10.1016/j.engstruct.2017.04.033

Nistor, M., Wiebe, R., & Stanciulescu, I. (2017). Relationship between Euler buckling and unstable equilibria of buckled beams. *International Journal of Non-Linear Mechanics*, *95*, 151–161. https://doi.org/10.1016/j.ijnonlinmec.2017.06.016

Rozylo, P., Ferdynus, M., Debski, H., & Samborski, S. (2020). Progressive Failure Analysis of Thin-Walled Composite Structures Verified Experimentally. *Materials*, 13(5), 1138.

Schilling, J. C., & Mittelstedt, C. (2020). Local buckling analysis of omega-stringer-stiffened composite panels using a new closed-form analytical approximate solution. *Thin-Walled Structures*, 147, 106534. https://doi.org/10.1016/j.tws.2019.106534

Shen, M.-Y., Chiou, Y.-C., Tan, C.-M., Wu, C.-C., & Chen, W.-J. (2020). Effect of Wall Thickness on Stress–Strain Response and Buckling Behavior of Hollow-Cylinder Rubber Fenders. *Materials*, 13(5), 1170.

Śledziewski, K., & Górecki, M. (2020). Finite Element Analysis of the Stability of a Sinusoidal Web in Steel and Composite Steel-Concrete Girders. *Materials*, 13(5), 1041.

Su, Y., Zhao, H., Liu, S., Li, R., Wang, Y., Wang, Y., Bian, J., & Huang, Y. (2019). Buckling of beams with finite prebuckling deformation. *International Journal of Solids and Structures*, 165, pp. 148-159. https://doi.org/10.1016/j.ijsolstr.2019.01.027

Timoshenko, S. P., & Gere, J. M. (2009). *Theory of elastic stability*. Courier Corporation.

Toledo, K. K., Kim, H.-S., Jeong, Y.-S., & Kim, I.-T. (2020). Residual Compressive Strength of Short Tubular Steel Columns with Artificially Fabricated Local Corrosion Damage. *Materials*, 13(4), 813.

Xu, R., & Wu, Y.-F. (2008). Free vibration and buckling of composite beams with interlayer slip by two-dimensional theory. *Journal of Sound and Vibration*, 313(3-5), pp. 875-890.

Zhu, X., Wang, Y., & Dai, H.-H. (2017). Buckling analysis of Euler–Bernoulli beams using Eringen's two-phase nonlocal model. *International Journal of Engineering Science*, 116, pp. 130-140. https://doi.org/10.1016/j.ijengsci.2017.03.008

Abstract: A new approach has been taken to the problem of straight and bent bar buckling, where bar buckling is considered as a function of axial displacement of one end. It was assumed that the length of a bar being buckled at any instant of buckling is the same as that of a straight bar, regardless of the size of axial displacement of one end of the bar. Based on energy equations, a formula was derived for the value of axial displacement of one bar end or buckling amplitude in the middle of bar length as a function of compressive force. The established relationships were confirmed by simulation tests using the finite element software Midas NFX and by experimental tests.

Keywords: buckling, Euler buckling, straight bar, bent bar, critical force